AutoJournal- Asean Journal of Automotive Technology

E- ISSN: 2710 - 5458

RESEARCH ARTICLE

MIXED CONVECTION BOUNDARY LAYER FLOW OF ENGINE OIL NANOFLUID ON A VERTICAL FLAT PLATE WITH VISCOUS DISSIPATION

M. K. A. Mohamed[a,*], H. R. Ong[a], M. Z. Salleh[b], B. Widodo[c]

[a] Faculty of Engineering, DRB-HICOM University of Automotive Malaysia, Peramu Jaya Industrial Area, 26607 Pekan, Pahang, MALAYSIA
[b] Applied & Industrial Mathematics Research Group, Faculty of Industrial Sciences and Technology, Universiti Malaysia Pahang, 26300 UMP Kuantan, Pahang, MALAYSIA
[c] Department of Mathematics, Institut Teknologi Sepuluh Nopember, 60111 Surabaya, INDONESIA

* Corresponding author: khairul.anuar@dhu.edu.my

ARTICLE HISTORY
Received: 30 June 2019
Accepted: 19 September

KEYWORDS
Convective boundary conditions
Engine oil nanofluid
Mixed convection
Vertical flat plate
Viscous dissipation

Abstract

The present study investigated the mixed convection boundary layer flow and heat transfer of engine oil nanofluid past a vertical flat plate which mimics the engine oil cooler assembly with the presence of velocity slip for lubricating effects, viscous dissipation and convective boundary conditions. The governing non-linear partial differential equations are first transformed into a system of ordinary differential equations using a similarity transformation before being solved numerically using the Runge-Kutta-Fehlberg (RKF45) method. Numerical solutions are obtained for the wall temperature, heat transfer coefficient and the skin friction coefficient as well as the temperature and velocity profiles. The features of the flow and heat transfer characteristics for copper Cu, silver Ag and titanium oxide TiO_2 engine oil nanofluid are analyzed and discussed. It is found that the TiO_2 engine oil nanofluid scored the lowest values of temperature and skin friction coefficient but provided the highest in heat transfer capabilities compared to Cu and Ag engine oil nanofluids. TiO_2 engine oil nanofluid is concluded as the best lubricant to suits the engine needs comparing to Cu and Ag engine oil nanofluid. It provided low friction and temperature which can prolong the engine component lifetime.

1.0 INTRODUCTION

The automotive manufacturers faced a challenge to build the high-efficiency engines which not only based on performance but also durability. The increase of engine output results to the needs of better engines lubricating system, in order to provide better friction reduction but also act as a heat transfer agent.

According to Wu (2011), the used of nanoparticles additives like *CuO*, TiO_2, *PbS* and *ZnS* can be used as additives to lubricants for reducing friction and wear. This type of fluid was first coin by Choi (1995) as a nanofluid. According to Kakaç and Pramuanjaroenkij (2009), nanofluid was proven in enhancing the thermal conductivity, viscosity, thermal diffusivity and convective heat transfer compared to its based fluids such as water and oil. Further, the used of nanofluid may reduce the chances of sedimentation and minimize the rate of erosion onto the surface (Lee et al., 1999, Das et al.,2006). By this, nearly no damaging on the surface which results to extend the lifetime onto the component.

Automotive industries used nanofluid as radiator coolant, brake fluid, fuel catalyst in order to improve the engine combustion as well as a smart fluid in battery. In medicine, nanofluid acted as a drug vehicle in cancer therapeutics (Wong and De Leon, 2010). The widely applications has influenced many researchers to investigate nanofluid characteristics as done by Tham et al. (2015), Zaraki et al. (2015), Abdolbaqi et al. (2016), Anwar et al. (2016), Azmi et al. (2016), Khan (2017), Kho et al. (2017) and Mohamed et al. (2017). Recently, Swalmeh et al. (2018), Yasin et al. (2019) Alkasasbeh et al. (2019) and Ishak et al. (2019) numerically investigated the free and the mixed convection boundary layer flow and heat transfer of a viscoelastic and micropolar nanofluid containing oxide nanoparticles over a stretching/shrinking sheet and solid sphere with the presence of velocity slip condition, magnetohydrodynamic (MHD), thermal radiation effect and Newtonian heating boundary conditions, respectively. The numerical solutions are obtained using finite difference method known as Keller-box method and Runge-Kutta-Fehlberg (RKF45) method with the aid of Matlab and Maple software.

In many numerical investigations practiced, the viscous dissipation effect is neglect. The viscous dissipation described as the process of converting the mechanical energy of downward flowing fluid into thermal and acoustical energy (Yirga and Shankar, 2015). Viscous dissipation effect usually presents in free convection with large decelerations from high rotating speeds and also in highly viscous flow with moderate velocity (Gebhart, 1962). Recent investigations on viscous dissipation effects including the works by Saidulu et al. (2018), Zokri et al. (2018), Jusoh et al. (2019) and Sharada and Shankar (2019).

Present study solve the slip flow and mixed convection on a vertical flat plate with viscous dissipation effect and convective boundary conditions to mimic the model of engine oil nanofluid flow and heat transfer in oil cooler assembly in modern engine. From the literature studies, this numerical study is never been reported hence the results published here are genuine.

2.0 MATHEMATICAL FORMULATIONS

Consider a steady incompressible engine oil nanofluid with ambient velocity, U_∞ and ambient temperature, T_∞ passes through the engine oil cooler assembly. The surface of the oil cooler is assumed as a vertical flat plate with surface temperature, T_w and there exist the velocity slip factor σ^* on a plate which represent the engine oil lubricating properties on the engines component surface. Gravity acceleration is represented by g and temperature in the boundary layer as T. It is further assumed that the plate is subjected to convective boundary conditions (CBC) which reflect to real convective heat transfer process between the plate and fluid. The physical model and coordinate system of this problem are shown in Figure 1. The proposed boundary layer equations are (Mohamed et al., 2013, Ramli et al., 2017, Mohamed et al., 2019):

$$\frac{\partial u}{\partial x}+\frac{\partial v}{\partial y}=0, \tag{1}$$

$$u\frac{\partial u}{\partial x}+v\frac{\partial u}{\partial y}=\nu_{nf}\frac{\partial^2 u}{\partial y^2}+\frac{(\rho\beta)_{nf}}{\rho_{nf}}g(T-T_\infty), \tag{2}$$

$$u\frac{\partial T}{\partial x}+v\frac{\partial T}{\partial y}=\frac{k_{nf}}{(\rho C_p)_{nf}}\frac{\partial^2 T}{\partial y^2}+\frac{\mu_{nf}}{(\rho C_p)_{nf}}\left(\frac{\partial u}{\partial y}\right)^2, \tag{3}$$

subjected to the boundary conditions

$$u=\sigma^*\frac{\partial u}{\partial y},\ v=0,\ -k_f\frac{\partial T}{\partial y}=-h_f(T_w-T)\ \text{at}\ y=0,$$

$$u\to U_\infty,\ T\to T_\infty\ \text{as}\ y\to\infty, \tag{4}$$

where u and v are the velocity components along the x and y directions, respectively. Further, h_f is the heat transfer coefficient, ν_{nf} is the kinematic viscosity of nanofluid, ρ_{nf} is the nanofluid density and α_{nf} is the thermal diffusivity of nanofluid, which can be expressed in terms of the properties of base fluid, nanoparticles and solid volume fraction ϕ as follows (Bachok et al., 2011, Khan et al., 2014):

$$\begin{gathered}\nu_{nf}=\frac{\mu_{nf}}{\rho_{nf}},\ \rho_{nf}=(1-\phi)\rho_f+\phi\rho_s,\\ \alpha_{nf}=\frac{k_{nf}}{\rho_{nf}(C_p)_{nf}},\ \mu_{nf}=\frac{\mu_f}{(1-\phi)^{2.5}},\\ \frac{k_{nf}}{k_f}=\frac{k_s+2k_f-2\phi(k_f-k_s)}{k_s+2k_f+\phi(k_f-k_s)},\\ (\rho\beta)_{nf}=(1-\phi)(\rho\beta)_f+\phi(\rho\beta)_s,\\ (\rho C_p)_{nf}=(1-\phi)(\rho C_p)_f+\phi(\rho C_p)_s,\end{gathered} \tag{5}$$

Note that k_{nf}, k_f and k_s are the thermal conductivity of the nanofluid, base fluid and nanoparticles, respectively while $(\rho C_p)_{nf}$ is the heat capacity of nanofluid.

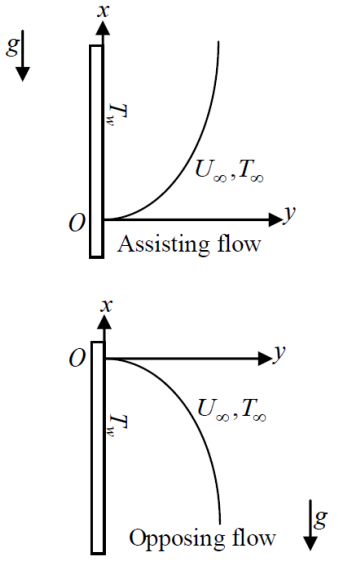

Figure 1. Physical model and the coordinate system

The non-linear partial differential Eqs. (1)-(3) contains many dependent variables which difficult to solve in dimensional. Therefore, the following similarity variables are applied:

$$\eta = \left(\frac{U_\infty}{2\nu_f x}\right)^{1/2} y,\ \psi = \left(2U_\infty \nu_f x\right)^{1/2} f(\eta),$$
$$\theta(\eta) = \frac{T - T_\infty}{T_w - T_\infty}, \tag{6}$$

where η, θ and ψ are non-dimensional similarity variable, temperature and stream function. The Eq. (1) is satisfied by definition of $u = \frac{\partial \psi}{\partial y}$ and $v = -\frac{\partial \psi}{\partial x}$, respectively. Next, the Eqs. (5) and (6) are substitute into Eqs. (2)-(3) which gives the following ordinary differential equations as follows:

$$\frac{1}{(1-\varphi)^{2.5}\left[1-\varphi+(\varphi\rho_s)/(\rho_f)\right]} f''' + ff'' - 2\frac{(1-\varphi)\rho_f + \varphi(\rho\beta)_s/\beta_f}{(1-\varphi)\rho_f + \varphi\rho_s}\lambda\theta = 0 \tag{7}$$

$$\frac{1}{\Pr}\frac{k_{nf}/k_f}{(1-\varphi)+\varphi(\rho C_p)_s/(\rho C_p)_f}\theta'' + f\theta' + \frac{Ec}{(1-\varphi)^{2.5}\left[(1-\varphi)+\varphi(\rho C_p)_s/(\rho C_p)_f\right]} f''^2 = 0, \tag{8}$$

where $\lambda = \frac{Gr}{\mathrm{Re}^2}$ is the buoyancy parameter, $Gr = \frac{g\beta_f (T_w - T_\infty)x^3}{\nu_f{}^2}$ is the Grashoff number, $\mathrm{Re} = \frac{U_\infty x}{\nu_f}$ is the Reynolds number, $\Pr = \frac{\nu_f (\rho C_p)_f}{k_f}$ is the Prandtl number and $Ec = \frac{(U_\infty)^2}{(C_p)_f (T_w - T_\infty)}$ is Eckert number. The transformed boundary conditions are

$$f(0) = 0,\ f'(0) = \sigma f''(0),\ -\theta'(0) = \gamma(1-\theta(0)),$$
$$f'(\eta) \to 1,\ \theta(\eta) \to 0 \text{ as } y \to \infty. \tag{9}$$

where $\sigma = \frac{\sigma^* \mu_f}{(1-\phi)^{2.5}}\left(\frac{U_\infty}{2\nu_f x}\right)^{1/2}$ and $\gamma = \frac{h_f}{k_f}\left(\frac{2\nu_f x}{U_\infty}\right)^{1/2}$ are the velocity slip parameter and conjugate parameter, respectively. In order that the similarity solution for Eqs. (7) to (9) exist, it is assumed (Aziz, 2009, Ishak, 2010, Makinde and Olanrewaju, 2010):

$$\beta_f = m_1 x^{-1}, h_f = m_2 x^{-1/2} \text{ and } \sigma^* = m_3 x^{1/2} \tag{10}$$

where m_1, m_2 and m_3 are constants. Note that the assumption in Eq. (10) is necessary for the Eqs. (7)-(9) to be independent of x. The physical quantity interest are the wall temperature $\theta(0)$, the heat transfer rate $-\theta'(0)$ and the skin friction coefficient C_f which given by

$$C_f = \frac{\tau_w}{\rho_f u_\infty^2}, \tag{11}$$

with surface shear stress $\tau_w = \mu_{nf}\left(\frac{\partial u}{\partial y}\right)_{y=0}$. Using the similarity variables in (6) gives

$$C_f\left(\mathrm{Re}/2\right)^{1/2} = \frac{f''(0)}{(1-\varphi)^{2.5}}. \tag{12}$$

which are referred as the reduced skin friction coefficient.

3.0 RESULTS AND DISCUSSION

The ordinary differential equations (8)-(10) subject to boundary conditions (12) are solved numerically using the proven Runge-Kutta-Fehlberg (RKF45) method. The small range of boundary layer thickness from 2 to 5 is sufficient to provide accurate numerical results. Six pertinent parameters namely as the Prandtl number $\Pr$, the buoyancy parameter λ, the Eckert number Ec, the velocity slip parameter σ, nanoparticles volume fraction ϕ and the conjugate parameter γ are considered. In addition, three types of nanoparticles which are copper Cu, silver Ag and titanium oxide TiO_2 with engine oil as a based fluid were tested. The thermophysical of engine oil and the nanoparticles are given in Table 1. Interestingly, at the end of this section, the conclusion can be made on which nanoparticles are most suitable to be employed as engines lubricant additive.

Table 1. Thermophysical properties of engine oil based fluid and nanoparticles

Physical Properties	Engine oil	Cu	Ag	TiO_2
ρ (kg/m³)	884	8933	10500	4250
C_p (J/kg·K)	1910	385	235	686.2
k(W/m·K)	0.144	400	429	8.9538
β (1/K)	0.0007	0.0000167	0.0000189	0.000009

In order to validate the suitability and precision of the method used, the comparison has been made. Table 2 shows the comparison values of $-\theta(0)/\sqrt{2}$ with previous results in Bataller (2008) and Roşca and Pop (2014) for the case of constant wall temperature (CWT). It is found that both tables provided the very good agreement. Hence, it is confident that the results presented in this study are accurate. Further,

Table 2. Comparison values of $-\theta'(0)/\sqrt{2}$ with previous studies for various values of $\Pr$ when $\lambda=\phi=\sigma=Ec=0, \gamma=\infty$ and $\gamma=1$.

$\Pr$	Roşca and Pop (2014)	Present		
	$-\theta'(0)/\sqrt{2}$	(CWT)	$\theta(0)$ (CBC)	$-\theta'(0)$ (CBC)
0.7	0.29268	0.29268	0.70726	0.29274
0.8	0.30691	0.30692	0.69733	0.30267
1	0.33205	0.33206	0.68045	0.31955
5	0.57668	0.57669	0.55079	0.44921
10	0.72814	0.72814	0.49267	0.50733
30		1.05133	0.40203	0.59797
50		1.24733	0.36180	0.63820
75		1.42804	0.33117	0.66883
100		1.57188	0.31027	0.68973

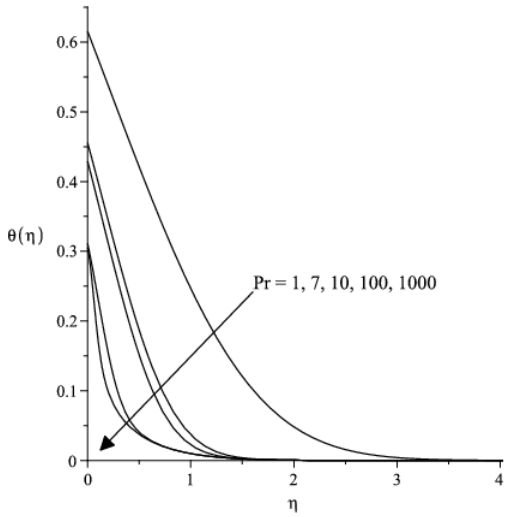

Figure 2. Temperature profiles $\theta(\eta)$ for various values of $\Pr$ when $Ec=0.1, \phi=0.01, \lambda=-0.5, \sigma=0.5$ and $\gamma=1$.

Table 2 also proposed the solution for wall temperature $\theta(0)$ and heat transfer coefficient $-\theta'(0)$ with respect to various values of Pr. It is observed that the increase in Pr results to a decrease in $\theta(0)$ while $-\theta'(0)$ increases. Physically, it can be interpreted that fluid with large value of Pr like engine oil will have a low temperature at the surface but with high heat transfer rate. This made the engine oil as a good fluid in protecting the engine component surface from heat while providing a good lubricating medium.

Next, Figure 2 to 20 illustrate the effects of pertinent parameter discussed on the temperature profiles $\theta(\eta)$, velocity profiles $f'(\eta)$ as well as variations on wall temperature $\theta(0)$ and reduced skin friction coefficient $C_f\left(\mathrm{Re}/2\right)^{1/2}$. The $\Pr$ is set as high as 100 to represent the engine oil characteristics as a based fluid. Noticed that the temperature profiles $\theta(\eta)$ and velocity profiles $f'(\eta)$ discussed from Figures 2 to 12 are calculated based on Cu nanoparticles properties which generally provided results regarding the effects of parameter applied for all nanoparticles considered.

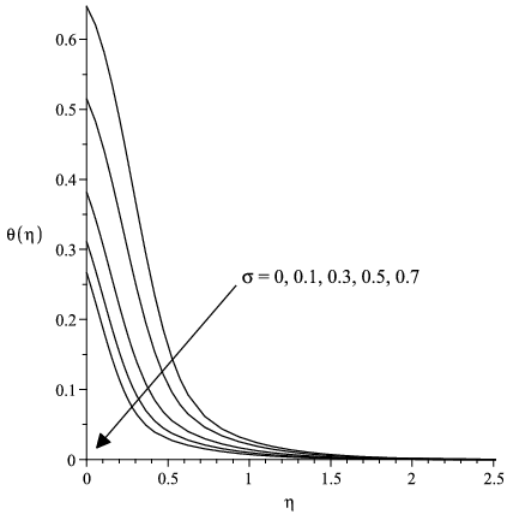

Figure 3. Temperature profiles $\theta(\eta)$ for various values of σ when $\Pr=100, Ec=0.1, \phi=0.01, \lambda=-0.5$ and $\gamma=1$.

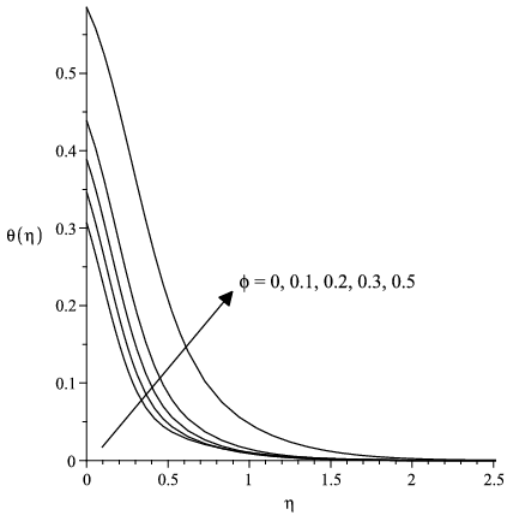

Figure 4. Temperature profiles $\theta(\eta)$ for various values of ϕ when $\Pr=100, Ec=0.1, \sigma=0.5, \lambda=-0.5$ and $\gamma=1$.

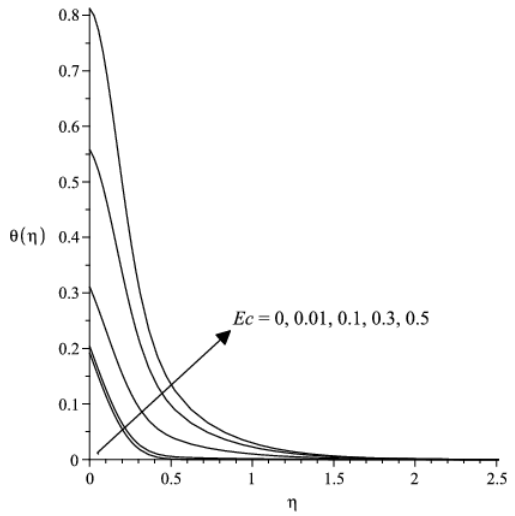

Figure 5. Temperature profiles $\theta(\eta)$ for various values of Ec when $\Pr = 100, \phi = 0.01,\ \sigma = 0.5, \lambda = -0.5$ and $\gamma = 1$.

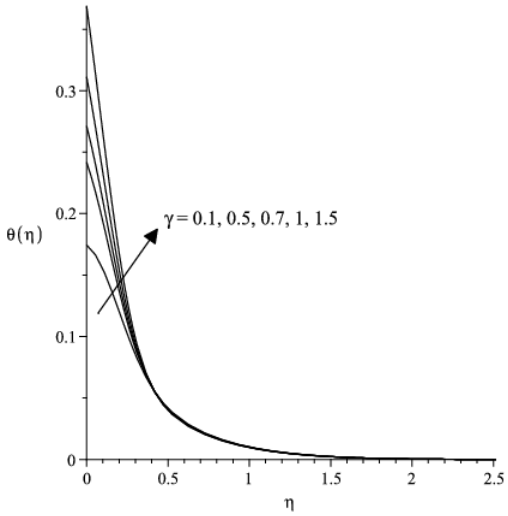

Figure 7. Temperature profiles $\theta(\eta)$ for various values of γ when $\Pr = 100, Ec = 0.1,\ \phi = 0.01, \lambda = -0.5$ and $\sigma = 0.5$

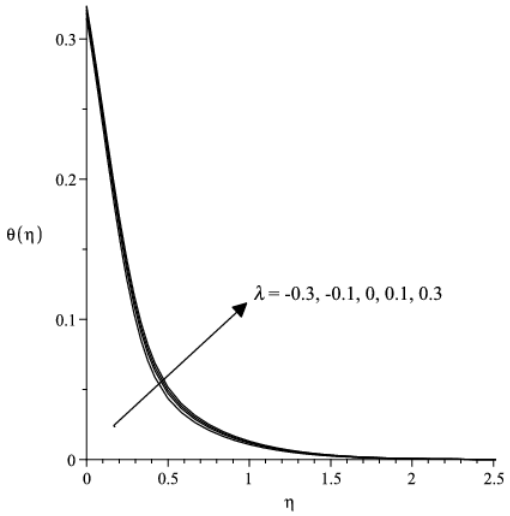

Figure 6. Temperature profiles $\theta(\eta)$ for various values of λ when $\Pr = 100, \phi = 0.01,\ Ec = 0.1, \sigma = 0.5$ and $\gamma = 1$.

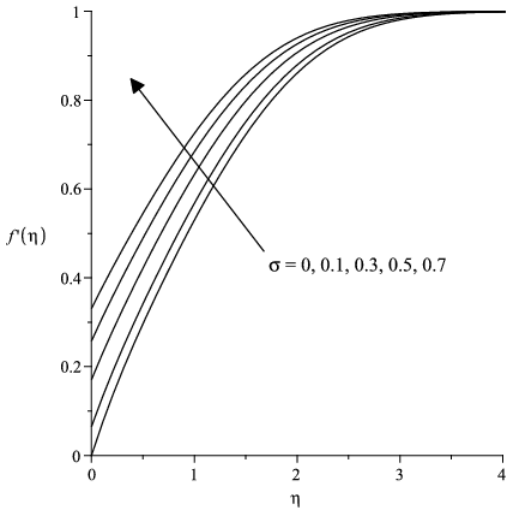

Figure 8. Velocity profiles $f'(\eta)$ for various values of σ when $\Pr = 100, Ec = 0.1,\ \phi = 0.01, \lambda = -0.5$ and $\gamma = 1$.

The temperature profiles $\theta(\eta)$ for various values of $\Pr, \sigma, \phi, \lambda, Ec$ and γ are shown in Figure 2 to 7, respectively. It is found that the increase in $\Pr$ and σ reduced the wall temperature as well as its thermal boundary layer thicknesses. Physically, the increase of $\Pr$ reduced the thermal diffusivity and this phenomenon leads to a decreasing energy ability that reduces the thermal boundary layer (Mohamed *et al.*, 2013). Meanwhile, the situation goes contrary for ϕ, λ, Ec and γ in Figures 4 to 7. As the parameter increases, the wall temperature also increases. The effect on wall temperature was large except for λ which gives nearly negligible effects both for temperature and the boundary layer thickness either for an assisting flow $(\lambda > 0)$ or opposing flow $(\lambda < 0)$.

Next, the increase in γ shows an increment in wall temperature but gives no effect on boundary layer thickness. It is worth mentioning here that from the boundary conditions (12), the heat transfer coefficient is inversely proportional to the wall temperature. It is the increase in wall temperature can be interpreted as a decrease in heat transfer coefficient.

Figures 8 to 12 illustrate the velocity profiles for various values of $\sigma, Ec, \Pr, \lambda$ and γ, respectively. From Figures 8 and 9, it is observed that the increase of σ and Ec raised the fluid velocity at the surface while decreasing a velocity boundary layer thickness. It is not surprise because the present of σ has disobey the no slip condition $(\sigma = 0)$ for fluid particles at the surface. This phenomenon has dragged the fluid particle from static to a certain velocity which then

contributes to the increase in fluid velocity overall in the boundary layer.

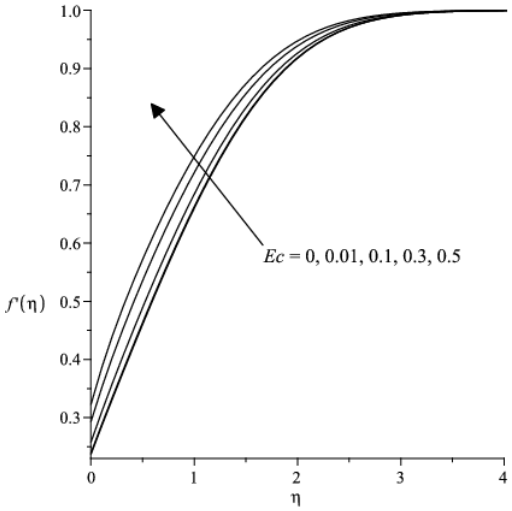

Figure 9. Velocity profiles $f'(\eta)$ for various values of Ec when $\Pr = 100, \phi = 0.01,\ \sigma = 0.5, \lambda = -0.5$ and $\gamma = 1$.

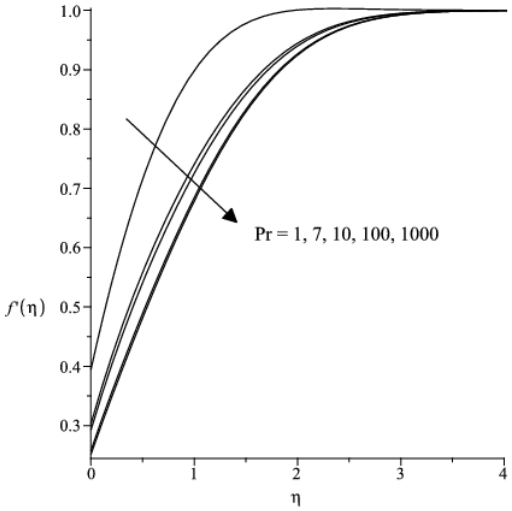

Figure 10. Velocity profiles $f'(\eta)$ for various values of $\Pr$ when $Ec = 0.1, \phi = 0.01,\ \lambda = -0.5, \sigma = 0.5$ and $\gamma = 1$.

Next, the increase in $\Pr$ and λ in Figures 10 and 11 has reduced the fluid velocity while the boundary layer thickness increases. The effects of $\Pr$ is more significant compared to λ as described in Figure 6 previously. Again, the buoyancy effect plays a very small role in fluid flow. Specifically, fluid with large value of $\Pr$ like oil usually is high viscosity fluid which therefore will have a low velocity but high in momentum compared to fluid with low $\Pr$ such as air and electrolyte. In Figure 12, the velocity profiles $f'(\eta)$ for various values of γ shows a unique curve which can be easily interpreted as this parameter gives no effects on velocity distribution as well as the boundary layer thicknesses. Since γ gives no effect on velocity distribution, the velocity gradient will also not affected thus results to no effects on skin friction coefficient.

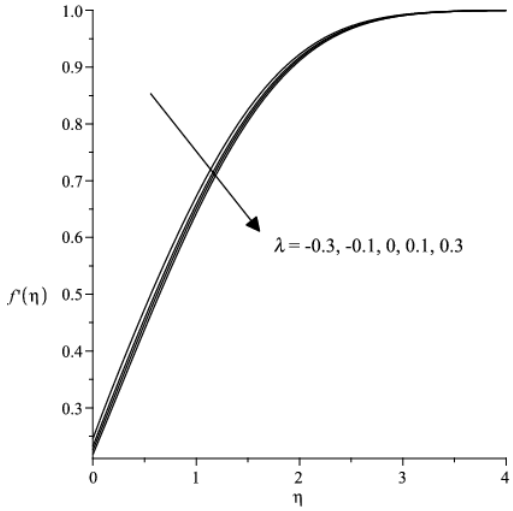

Figure 11. Velocity profiles $f'(\eta)$ for various values of λ when $\Pr = 100, \phi = 0.01,\ Ec = 0.1, \sigma = 0.5$ and $\gamma = 1$.

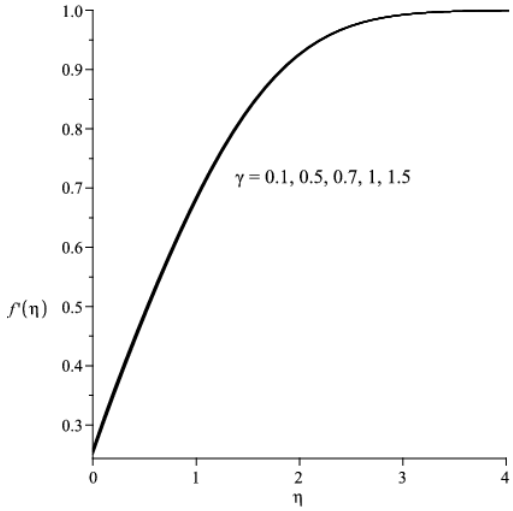

Figure 12. Velocity profiles $f'(\eta)$ for various values of γ when $\Pr = 100, Ec = 0.1,\ \phi = 0.01, \lambda = -0.5$ and $\sigma = 0.5$

In order to investigate the effects of parameters on various nanofluid engine oil, Figure 13 to 20 are illustrates. Figure 13 to 16 show the variation of wall temperature $\theta(0)$ with various values of ϕ, λ, Ec and σ, on Cu, Ag and TiO_2 engine oil nanofluid, respectively. From figures, it is found that the Ag engine oil nanofluid produced the highest wall temperature $\theta(0)$ compared to Cu and TiO_2. The result is more significant as ϕ increases. Physically, Ag nanoparticles has higher thermal conductivity and thermal expansion coefficient while specific heat capacity lower than Cu and TiO_2. This contributed to the increase in temperature at the surface and on the other hand reduced the heat transfer coefficient

between fluid and surface. In Figure 15, it is noticed that the increase in viscous dissipation which represent by Ec raised the temperature linearly but give no significant effect on nanoparticles employed in engine oil nanofluid. Meanwhile, the increase in slip velocity σ had reduced the values of $\theta(0)$ and gave very small effect on nanoparticles employed as in Figure 15.

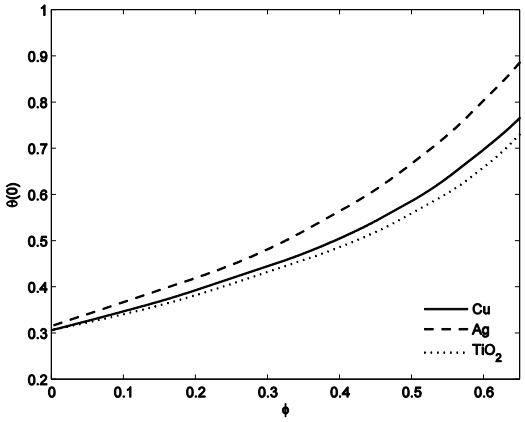

Figure 13. Variation of $\theta(0)$ for various nanoparticles along ϕ when $\Pr = 100, Ec = 0.1,\ \sigma = 0.5, \lambda = -0.5$ and $\gamma = 1$.

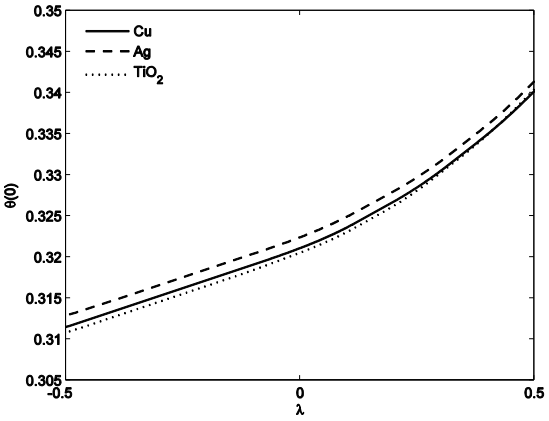

Figure 14. Variation of $\theta(0)$ for various nanoparticles along λ when $\Pr = 100, \phi = 0.01,\ Ec = 0.1, \sigma = 0.5$ and $\gamma = 1$.

Lastly, Figures 17 to 20 show the variation of reduced skin friction coefficient $C_f\left(\mathrm{Re}/2\right)^{1/2}$ for various values of ϕ, λ, Ec and σ, respectively. From Figures 17 and 18, it is found that the increase of ϕ and Ec raised the friction between plate surface and fluid. Physically, the increase in ϕ provide large volume of nanoparticles in fluid which caused more friction between surface and nanoparticles and therefore damaged the surface especially the surface of engine components. Further, the increase in ϕ are not recommended because it contributed clogging especially in narrow channel such as turbocharged piping and oil hose in modern engine.

In considering the effects of λ on $C_f\left(\mathrm{Re}/2\right)^{1/2}$, from Figure 19, it is found that the increase of λ in assisting flow $(\lambda > 0)$ results to a reducing values of $C_f\left(\mathrm{Re}/2\right)^{1/2}$. Noticed that the trends is contrary in opposing flow $(\lambda < 0)$.

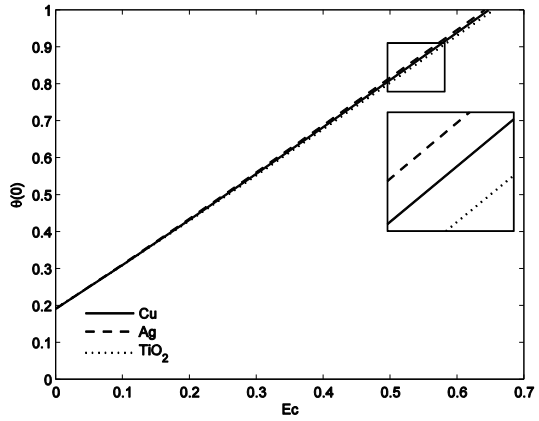

Figure 15. Variation of $\theta(0)$ for various nanoparticles along Ec when $\Pr = 100, \phi = 0.01,\ \sigma = 0.5, \lambda = -0.5$ and $\gamma = 1$.

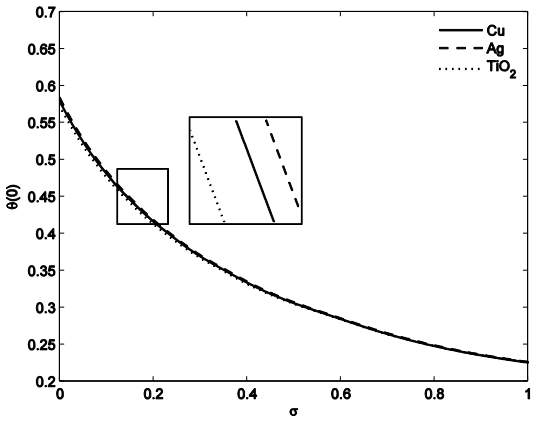

Figure 16. Variation of $\theta(0)$ for various nanoparticles along σ when $\Pr = 100, Ec = 0.1,\ \phi = 0.01, \lambda = -0.5$ and $\gamma = 1$.

On the other hand, the present of velocity slip effect has reduced the values of $C_f\left(\mathrm{Re}/2\right)^{1/2}$. It is realistic since the velocity slip had reduced a difference between fluid flow velocity outside the boundary layer with fluid at the surface therefore reduced the velocity gradient as well as the skin friction coefficient. In overall, it can be suggested that the Ag engine oil nanofluid produced highest skin friction coefficient $C_f\left(\mathrm{Re}/2\right)^{1/2}$ while TiO_2 scored the lowest.

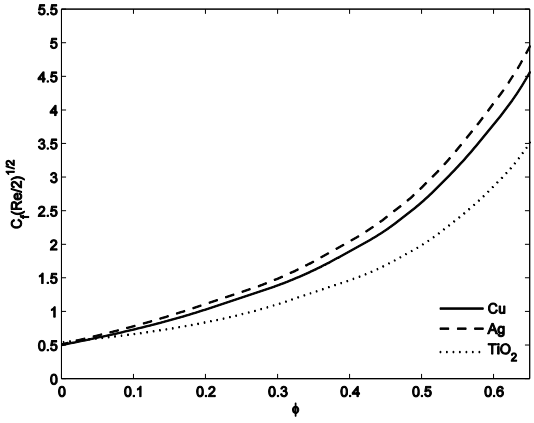

Figure 17. Variation of $C_f(\mathrm{Re}/2)^{1/2}$ for various nanoparticles along ϕ when $\mathrm{Pr}=100, Ec=0.1,$ $\sigma=0.5, \lambda=-0.5$ and $\gamma=1.$

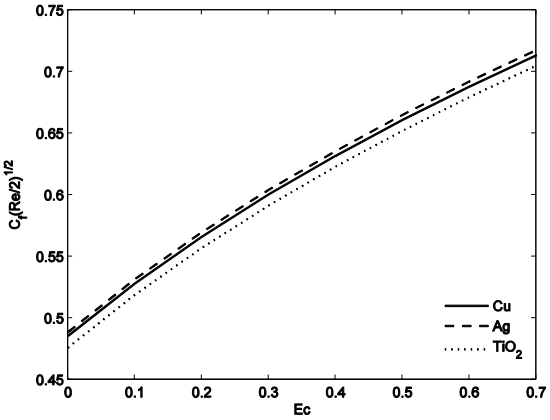

Figure 18. Variation of $C_f(\mathrm{Re}/2)^{1/2}$ for various nanoparticles along Ec when $\mathrm{Pr}=100, \phi=0.01,$ $\sigma=0.5, \lambda=-0.5$ and $\gamma=1.$

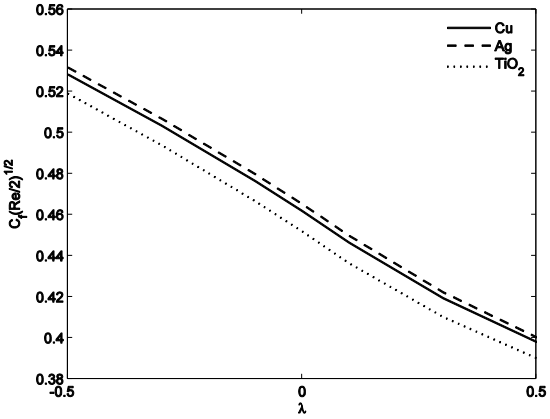

Figure 19. Variation of $C_f(\mathrm{Re}/2)^{1/2}$ for various nanoparticles along λ when $\mathrm{Pr}=100, \phi=0.01,$ $Ec=0.1, \sigma=0.5$ and $\gamma=1.$

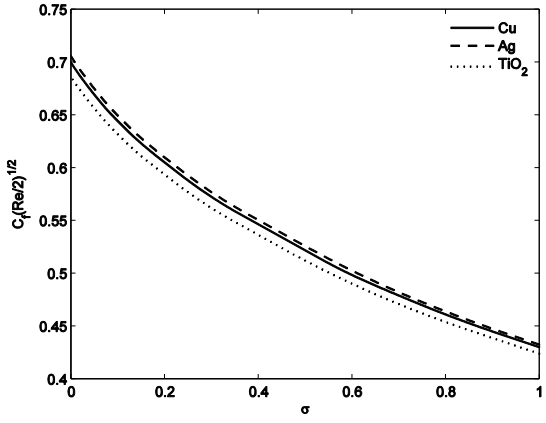

Figure 20. Variation of $C_f(\mathrm{Re}/2)^{1/2}$ for various nanoparticles along σ when $\mathrm{Pr}=100, Ec=0.1,$ $\phi=0.01, \lambda=-0.5$ and $\gamma=1.$

In thermal cooling systems especially in modern engine, the engine oil employed must have low friction and temperature but high in heat transfer capabilities. From numerical calculations and figures, the TiO_2 engine oil nanofluid is the best lubricant to suits the engine needs. Ag engine oil nanofluid is not recommended since it produced high temperature at surface, highly in friction between fluid and component surface which can cause damaging and also low in heat transfer capabilities.

4.0 CONCLUSION

The present study has solved the mathematical model of engine oil nanofluid flow and heat transfer on a vertical flat plate with slip effects, viscous dissipation and convective boundary conditions. The effects of Prandtl number Pr, the buoyancy parameter λ, the Eckert number Ec, the velocity slip parameter σ, nanoparticle volume fraction ϕ and the conjugate parameter γ with three different nanoparticles namely as copper Cu, silver Ag and titanium oxide TiO_2 on the temperature and velocity profiles, the variation of wall temperature and reduced skin friction coefficient are discussed in details.

As a conclusion, the increase in σ and Pr reduced the temperature profiles $\theta(\eta)$ as well as the thermal boundary layer thicknesses while ϕ and Ec does contrary. In considering the velocity profiles $f'(\eta)$, as σ and ϕ increases, the velocity at surface increases but the velocity boundary layer thickness decreases. Besides, it is found that changes in λ and γ gives no effect on thermal and velocity boundary layer thicknesses.

From the numerical computation, the increase of σ and λ in assisting flow $(\lambda > 0)$ had reduced the skin friction coefficient which in turn reduced the component surface friction and hence prolong the lifetime of engine components. Futhermore, it is good to keep the ϕ in a very small value such as 1% in order to reduced clogging.

Lastly, in comparing the nanoparticles' performance in heat transfer capabilities and friction, it is found that the TiO_2 engine oil nanofluid scored the lowest values of temperature and skin friction coefficient but provided the highest in heat transfer capabilities compared to Cu and Ag engine oil nanofluids. In automotive, the most important aspect in the engine lubricating system is to provide low friction and temperature which can prolong the engine component lifetime. Therefore, it is concluded that TiO_2 engine oil nanofluid as the best lubricant to suit the engine needs if comparing to Cu and Ag .

Acknowledgement

The authors would like to thank the DRB-HICOM University of Automotive Malaysia and Universiti Malaysia Pahang for the financial, facilities and moral support.

References

Abdolbaqi, M. K., Sidik, N. A. C., Aziz, A., Mamat, R., Azmi, W., Yazid, M. N. A. W. M. & Najafi, G. 2016. An experimental determination of thermal conductivity and viscosity of BioGlycol/water based TiO 2 nanofluids. *International Communications in Heat and Mass Transfer* 77: 22-32.

Alkasasbeh, H. T., Swalmeh, M. Z., Hussanan, A. & Mamat, M. 2019. Effects Of Mixed Convection On Methanol And Kerosene Oil Based Micropolar Nanofluid Containing Oxide Nanoparticles. *CFD Letters* 11(1): 55-68.

Anwar, M. I., Shafie, S., Kasim, A. R. M. & Salleh, M. Z. 2016. Radiation effect on mhd stagnation-point flow of a nanofluid over a nonlinear stretching sheet with convective boundary condition. 47(9): 797-816.

Aziz, A. 2009. A similarity solution for laminar thermal boundary layer over a flat plate with a convective surface boundary condition. *Communications in Nonlinear Science and Numerical Simulation* 14(4): 1064-1068.

Azmi, W. H., Abdul Hamid, K., Usri, N. A., Mamat, R. & Mohamad, M. S. 2016. Heat transfer and friction factor of water and ethylene glycol mixture based TiO2 and Al2O3 nanofluids under turbulent flow. *International Communications in Heat and Mass Transfer* 76: 24-32.

Bachok, N., Ishak, A. & Pop, I. 2011. Stagnation point flow over a stretching/shrinking sheet in a nanofluid. *Nanoscale Research Letter* 6.

Bataller, R. C. 2008. Radiation effects in the Blasius flow. *Applied Mathematics and Computation* 198: 333-338.

Choi, S. U. S. 1995. Enhancing thermal conductivity of fluids with nanoparticles. *American Society of Mechanical Engineers* 231: 99-105.

Das, S. K., Choi, S. U. S. & Patel, H. E. 2006. Heat Transfer in Nanofluids—A Review. *Heat Transfer Engineering* 27(10): 3-19.

Gebhart, B. 1962. Effects of viscous dissipation in natural convection. *Journal of Fluid Mechanics* 14(02): 225-232.

Ishak, A. 2010. Similarity solutions for flow and heat transfer over a permeable surface with convective boundary condition. *Applied Mathematics and Computation* 217(2): 837-842.

Ishak, N., Hussanan, A., Mohamed, M. K. A., Rosli, N. & Salleh, M. Z. 2019. Heat and mass transfer flow of a viscoelastic nanofluid over a stretching/shrinking sheet with slip condition. *AIP Conference Proceedings* 2059(1): 020011.

Jusoh, R., Nazar, R. & Pop, I. 2019. Magnetohydrodynamic Boundary Layer Flow and Heat Transfer of Nanofluids Past a Bidirectional Exponential Permeable Stretching/Shrinking Sheet With Viscous Dissipation Effect. *Journal of Heat Transfer* 141(1): 012406.

Kakaç, S. & Pramuanjaroenkij, A. 2009. Review of convective heat transfer enhancement with nanofluids. *International Journal of Heat and Mass Transfer* 52(13–14): 3187-3196.

Khan, I. 2017. Shape effects of MoS2 nanoparticles on MHD slip flow of molybdenum disulphide nanofluid in a porous medium. *Journal of Molecular Liquids* 233: 442-451.

Khan, Z. H., Khan, W. A., Qasim, M. & Shah, I. A. 2014. MHD stagnation point ferrofluid flow and heat transfer toward a stretching sheet. *IEEE Transactions on Nanotechnology* 13(1): 35-40.

Kho, Y. B., Hussanan, A., Mohamed, M. K. A., Sarif, N. M., Ismail, Z. & Salleh, M. Z. 2017. Thermal radiation effect on MHD Flow and heat transfer analysis of Williamson nanofluid past over a stretching sheet with constant wall temperature. *Journal of Physics: Conference Series* 890(1): 1-6.

Lee, S., Choi, S. U. S., Li, S. & Eastman, J. A. 1999. Measuring thermal conductivity of fluids containing oxide nanoparticles. *Journal of Heat Transfer* 121(2): 280-289.

Makinde, O. D. & Olanrewaju, P. O. 2010. Buoyancy Effects on Thermal Boundary Layer Over a Vertical Plate With a Convective Surface Boundary Condition. *Journal of Fluids Engineering* 132(4): 0445021-0445024.

Mohamed, M. K. A., Ismail, N. A., Hashim, N., Shah, N. M. & Salleh, M. Z. 2019. MHD Slip Flow and Heat Transfer on Stagnation Point of a Magnetite (Fe3O4) Ferrofluid towards a Stretching Sheet with Newtonian Heating. *CFD Letters* 11(1): 17-27.

Mohamed, M. K. A., Noar, N. A. Z., Salleh, M. Z. & Ishak, A. 2017. Slip flow on stagnation point over a stretching sheet in a viscoelastic nanofluid. *AIP Conference Proceedings* 1830(1): 020015.

Mohamed, M. K. A., Salleh, M. Z., Nazar, R. & Ishak, A. 2013. Numerical investigation of stagnation point flow over a stretching sheet with convective boundary conditions. *Boundary Value Problems* 2013(1): 1-10.

Ramli, N., Ahmad, S. & Pop, I. 2017. Slip effects on MHD flow and heat transfer of ferrofluids over a moving flat plate. *AIP Conference Proceedings* 1870(1): 040015.

Roşca, N. C. & Pop, I. 2014. Unsteady boundary layer flow of a nanofluid past a moving surface in an external uniform free stream using Buongiorno's model. *Computers & Fluids* 95: 49-55.

Saidulu, N., Gangaiah, T. & Lakshmi, A. V. 2018. Inclined Magnetic Field and Viscous Dissipation Effects on Tangent Hyperbolic Nanofluid Flow with Zero Normal Flux of Nanoparticles at the Stretching Surface. *European Journal of Advances in Engineering and Technology* 5(3): 142-150.

Sharada, K. & Shankar, B. 2019. MHD Stagnation Point Flow of a Micropolar Fluid Through a Porous Medium Over an Exponentially Stretching Sheet with Convective Boundary Condition, Viscous Dissipation. *Journal of Nanofluids* 8(2): 394-398.

Swalmeh, M. Z., Alkasasbeh, H. T., Hussanan, A. & Mamat, M. 2018. Heat transfer flow of Cu-water and Al2O3-water micropolar nanofluids about a solid sphere in the presence of natural convection using Keller-box method. *Results in Physics* 9: 717-724.

Tham, L., Nazar, R. & Pop, I. 2015. Mixed convection flow over a horizontal circular cylinder with constant heat flux embedded in a porous medium filled by a nanofluid: Buongiorno–Darcy model. *Heat and Mass Transfer* 52(9): 1983-1991.

Wong, K. V. & De Leon, O. 2010. Applications of Nanofluids: Current and Future. *Advances in Mechanical Engineering* 2: 519659.

Yasin, S. H. M., Mohamed, M. K. A., Ismail, Z., Widodo, B. & Salleh, M. Z. 2019. Numerical Solution on MHD Stagnation Point Flow in Ferrofluid with Newtonian Heating and Thermal Radiation Effect. *CFD Letters* 11(2): 21-31.

Yirga, Y. & Shankar, B. 2015. MHD flow and heat transfer of nanofluids through a porous media due to a stretching sheet with viscous dissipation and chemical reaction effects. *International Journal for Computational Methods in Engineering Science and Mechanics* 16(5): 275-284.

Zaraki, A., Ghalambaz, M., Chamkha, A. J., Ghalambaz, M. & De Rossi, D. 2015. Theoretical analysis of natural convection boundary layer heat and mass transfer of nanofluids: Effects of size, shape and type of nanoparticles, type of base fluid and working temperature. *Advanced Powder Technology* 26(3): 935-946.

Zokri, S. M., Arifin, N. S., Mohamed, M. K. A., Kasim, A. R. M., Mohammad, N. F. & Salleh, M. Z. 2018. Mathematical Model of Mixed Convection Boundary Layer Flow over a Horizontal Circular Cylinder Filled in a Jeffrey Fluid with Viscous Dissipation Effect. *Sains Malaysiana* 47(7): 1607-1615.